Research Academy for Young Scientists

Quantitative Cardiac T1ρ MRI: Segmentation and Multi-modal Comparison

Ana Kostic
anakostic5@yahoo.com

under the direction of
Pontus Pandurevic, *PhD Student*
Karolinska Institutet
Department of Molecular Medicine and Surgery

July 8, 2026

*

Abstract

Magnetic Resonance Imaging can image the human body, and, combined with contrast-agent injection, aids in diagnosing diseases, such as myocardial fibrosis. This study investigates how contrast-free maps $T1\rho$ and T2, and contrast-enhanced maps ECV and LGE relate to each other in what they detect. This can indicate if $T1\rho$ is robust enough to substitute for contrast agents, which is valuable since contrast agents can be dangerous to patients with kidney disease [1]. Elevated values (elevations) above the healthy range may indicate myocardial fibrosis [2]. Cardiac Magnetic Resonance Images of 41 patients were marked and segmented to extract the left ventricular myocardium. The myocardium was semi-automatically segmented to find mean values per segment. Using regions of interest, the number of times $T1\rho$ detected elevations, that LGE regions of interest already had, was counted. The correlation was stronger between T2 and $T1\rho$ scatter plots than for ECV vs. $T1\rho$, and ECV vs. T2. Additionally, 85% of $T1\rho$ slices detected elevations that LGE slices also found, which makes $T1\rho$ appear to be a promising alternative to LGE. In conclusion, the low correlations in the interval -0.5 $<$ r $<$ 0.5 indicate that maps detect elevations differently. $T1\rho$ correlated weakly with ECV, therefore, it needs more statistical evidence before it can fully replace contrast-based maps, even though $T1\rho$ detected 85% of elevations identified by LGE. The weak correlations could have been caused by outliers inadvertently included in the segmentation. In the future, apical slices could have been excluded since they contained more blood than other slices. Moreover, a larger margin around the left ventricular myocardium should be excluded during segmentation.

Acknowledgements

First and foremost, I would like to offer my deepest gratitude to Beijerstiftelsen, Jacob Wallenbergs Stiftelse and Hierta-Retzius Stipendiefond for supporting Rays. I also sincerely thank Rays, its board and this year's Rays organizers Maya Hagbok, Vic Kowalik, Marie Delort and Alicia Svensson for creating an environment where I could focus on science. In addition, I was able to get to know people who share the same passion for science as I do. I also thank the Rays organizers for the insightful lectures they held during the program, along with the feedback and advice that made conducting this research and writing this report possible.

Secondly, I also extend my heartfelt gratitude to my supervisor, Pontus Pandurevic, for excellent guidance and invaluable feedback I received during this project. I especially appreciate his clear communication and availability throughout the entire project, even outside the standard mentorship weeks.

Thirdly, I am deeply grateful to the xRays Albert Meurling Wipf and Kasper Johansson, who read my report in great detail and gave meticulous feedback on it. Their advice greatly improved my report to what is it today.

Fourthly, I sincerely thank my teachers Katarina Roxström Lindquist and Niklas Schild for writing me letters of recommendation. Without them, I may not have had the wonderful opportunity of attending Rays and conducting this project.

Last, but not least, I am extremely grateful for the love and support my family and close friends have provided me with during Rays. They have always cheered me on and believed in me, which I sincerely appreciate.

Contents

1 Introduction

Myocardial fibrosis is a cardiac disease where scar tissue forms in the heart muscle (myocardium) after myocardial injuries, such as an infarction. The scar tissue can lead to stiffening of the myocardium and heart failure. [3]

Myocardial fibrosis can be diagnosed through images produced by Magnetic Resonance Imaging (MRI). Specifically, an MRI of the heart is called Cardiovascular Magnetic Resonance (CMR).

Different measurements in an MRI yield different maps, with varying robustness in diagnosing myocardial fibrosis. Late gadolinium-enhanced imaging (LGE) is a valid clinical reference for diagnosing this disease [4]. It involves injection of a gadolinium-based contrast agent to increase tissue contrast. The issue with contrast agents is the risks it has for certain groups [5, 1, 6], which is why an alternative method is needed.

$T1\rho$ is a promising contrast-free technique to improve diagnosis of myocardial fibrosis. However, further evidence is needed to support its effectiveness [7]. In this study, its sensitivity to detecting myocardial fibrosis will be compared to contrast-based methods, such as LGE, and currently standard contrast-free methods.

1.1 Magnetic Resonance Imaging

Magnetic Resonance Imaging (MRI) uses a strong, static magnetic field between 0.5 and 7 Tesla (T) [8] and radiofrequency (RF) pulses as a non-invasive way to see inside the body. This static magnetic field is referred to as B_0 [9]. The MR images can be displayed as slices, which are 2D cross-sections of the 3D mapping.

MR images can be mapped using different measurements, such as $T2$ and T1ρ, which are all time measurements. These time measurements are based on the alignment of the precession of spin of hydrogen nuclei. Hydrogen nuclei are bound in molecules inside the body, such as water and macromolecules [8]. At first, the hydrogen nuclei are aligned parallel to $\vec{B_0}$ [9], the direction of the static magnetic field. After additional magnetization by RF pulses, the measurements differ depending on tissue, which enables tissue differentiation. The differentiation between tissues is based on the presence of hydrogen nuclei in

their respective chemical environments, depending on how ratios of water and molecules vary between tissues. MRI uses these measurements as contrast to display contours of organs. [8]

T1 is the longitudinal relaxation time [9], i.e., the time it takes for the precession of hydrogen nuclei to realign with $\vec{B_0}$, after being excited by an RF pulse [8]. T1 can be used to diagnose diffuse myocardial fibrosis [10].

T2 is the relaxation time in the transverse component of the net magnetization. Since the hydrogen nuclei are each in their respective environments, they do not experience the same magnetic field and do not precess at the same frequency it takes to preserve the transverse component. Therefore, the transverse component decays when the spins dephase and that decay is called T2 [8]. T2 yields higher values when water volume increases, which can indicate inflammation [11]. This increase in fluid within tissue, also known as edema, is often present in myocardial diseases [12].

$T1\rho$, like T1, also measures a longitudinal relaxation time, but against a different magnetic field. An RF pulse tips the net magnetization among the hydrogen nuclei by 90 degrees sideways, into the transverse plane. After that, a spin-lock RF pulse of amplitude B_1 is used to position the spins into transverse plane. $T1\rho$ is the time measured for relaxation within the transverse plane, as the amplitude of B_1 decreases and the spins dephase, as is the case in T2. Another RF pulse rotates the spins of the hydrogen nuclei back into the longitudinal plane, $\vec{B_0}$. [7]

To achieve greater signal to noise ratio (SNR) and greater tissue contrast in CMRs, the patient may be injected with a contrast agent. One example is gadolinium chelate-based contrast agents (GBCA) [6]. The GBCA can be used for Late gadolinium-enhanced imaging (LGE) to diagnose myocardial fibrosis [2]. LGE is a valid way to establishing this diagnosis [4].

The extracellular volume fraction (ECV) of the myocardium can be mapped to diagnose myocardial fibrosis [13]. This can be combined with a contrast agent, as in this study.

Figure 1 displays the above-mentioned maps: T1, T2, $T1\rho$, LGE and ECV. Each image

represents an identical slice, but mapped differently.

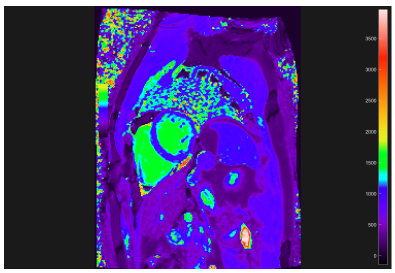

(a) T1

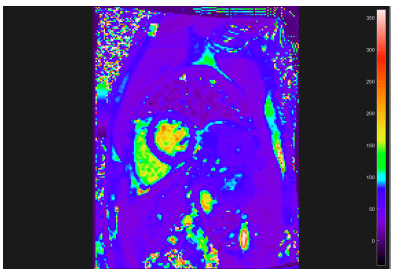

(b) T2

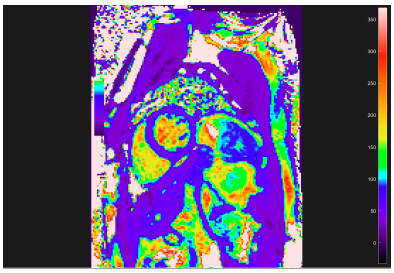

(c) $T1\rho$

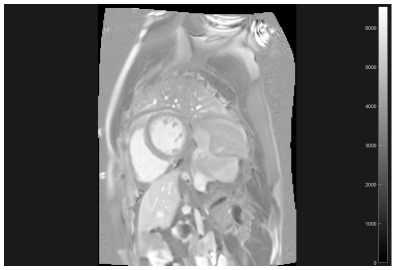

(d) LGE

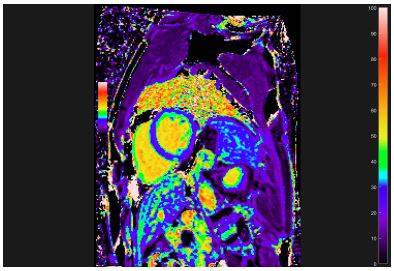

(e) ECV

Figure 1: The images above show the same cross-section slice of the short axis of the heart in the center of the leftmost vertical third of each image. The ring shape shows the myocardium. In T1, T2, $T1\rho$ and ECV maps, at their current contrast and brightness settings, the ring shape is purple. For LGE, it is light grey. Each image represents a different map: (a) for T1, (b) for T2, (c) for $T1\rho$, (d) for LGE, (e) for ECV. On the right side of each image a color bar is displayed, with marked values for each color.

1.2 Cardiac Anatomy

The American Heart Association (AHA) describes standard nomenclature for left ventricular (LV) segmentation. The LV is divided into three layers, sliced parallel to the short-axis of the heart, starting from above: basal, mid-cavity and apical. Subsequently, each part is divided into smaller portions, as presented in Figure 2. In a short axis cross-sectional MR image, the heart has the same shape shown in Figure 3, where the septum divides the right and left ventricles. The AHA model uses 17 segments, but this study will exclude apex (segment 17), which yields 16 segments. [14]

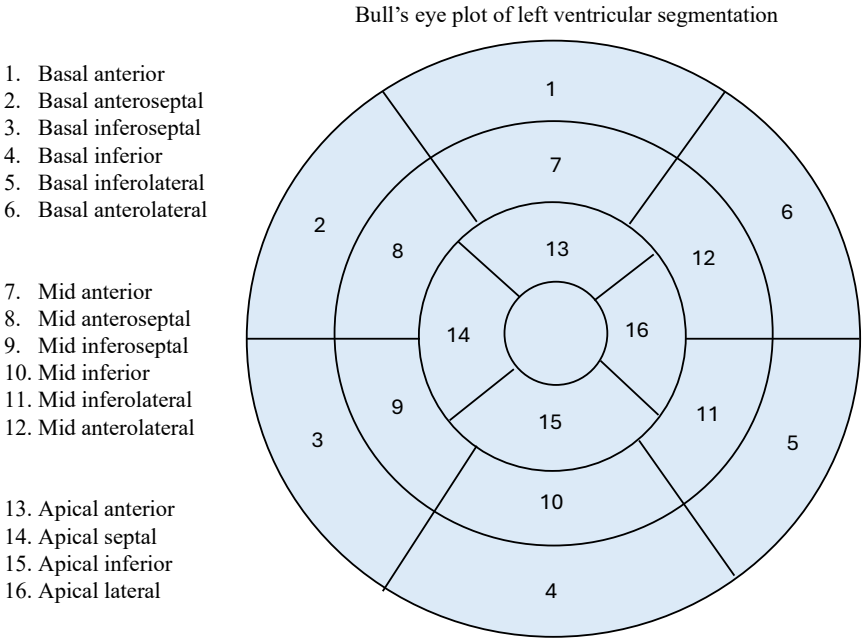

Figure 2: The figure shows a bull's-eye plot over the 16 segments of the left ventricle, based on the 17-segment AHA-model. Basal and mid parts are split into six smaller subparts: anterior, anteroseptal, inferoseptal, inferolateral and anterolateral. The apical part is split into four parts: anterior, septal, inferior and lateral. [14]

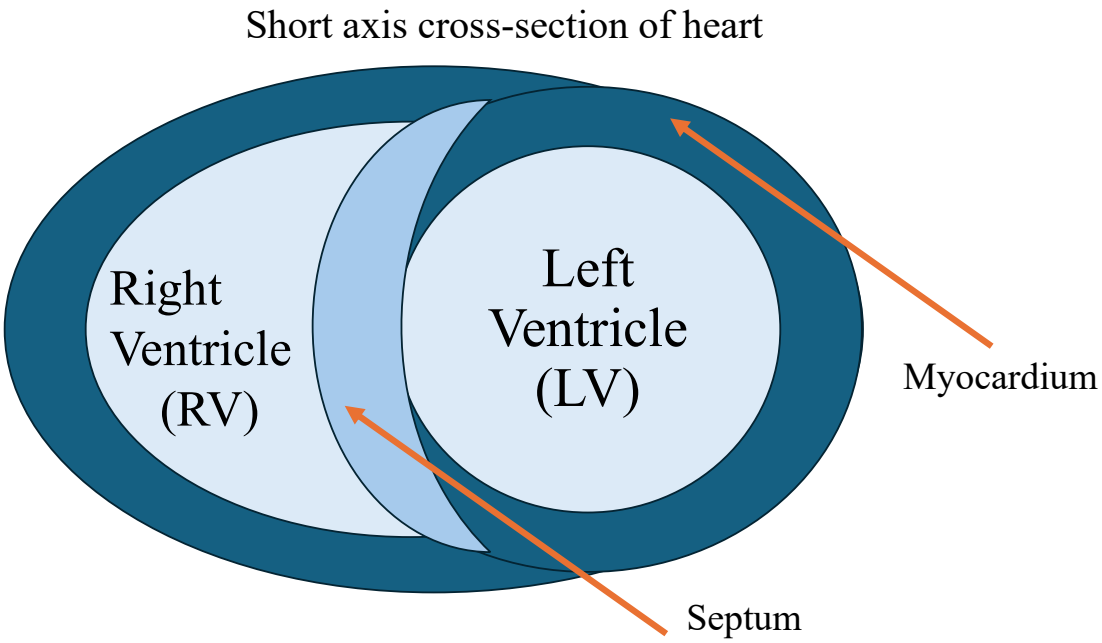

Figure 3: The figure shows an illustration of the cross-sectional short axis of heart. Left ventricle is on the right, and the right ventricle to the left. [14]

The LV is a chamber in the heart that acts as the main blood pump. After cardiac injury, such as from a myocardial infarction, the left ventricle may change geometrically and functionally, for example from formed fibrotic tissue. This change can lead to heart failure and death. [5]

1.3 Myocardial Fibrosis

Extracellular matrix expansion [7], creates an excessive accumulation of collagen in the myocardium. This collagen build-up characterizes the disease myocardial fibrosis. Specifically, the fibrotic tissue, also called scar tissue, appears highlighted by increased relaxation-time values [2]. Since T1ρ is particularly sensitive to water-macromolecule interactions, it shows increased values when extracellular matrix is present [7]. This can be used to detect the microstructural and biochemical changes in tissue [15].

There are two main types of myocardial fibrosis: focal and diffuse. Focal myocardial fibrosis can happen after myocyte necrosis after an infarction [16]. Diffuse myocardial fibrosis is reversible, therefore making it an interesting disease to target a treatment for [10]. This study focuses on focal myocardial fibrosis.

1.4 Reference values for Tissue in CMRs

When the magnetic field strength is 1.5T, there are fixed values that represent healthy myocardial tissue. For $T1\rho$, the normal values are 54.2±2.56 ms [17], as presented at ISMRM May 2026. Meanwhile, the normal T2 values are 52.18±3.4 ms [11]. For contrast-enhanced ECV, normal values lie between 20.4% and 30.4% [13]. As previously mentioned, maps yield elevated measurements (elevations) when collagen is present in myocardial fibrosis [2].

1.5 Issues with GBCA

The disadvantage of injection of contrast agents may lead to allergic reactions in rare cases. In addition to that, GBCA are not recommended for pregnant patients [6], while the agents may cause nephrogenic systemic fibrosis in patients with renal diseases [1]. Additionally, GBCA injections can lead to minor side effects, such as nausea and headaches [1]. To minimize patient discomfort and include the groups unable to safely receive GBCA injection in MRI diagnosis, a different, contrast agent-free method is needed.

1.6 Aim of study

The aim of this study is to investigate the relationship between MRI maps to evaluate $T1\rho$ against conventional techniques used in clinical settings. Myocardial fibrosis is the main use case for this study. This investigation aims to determine whether $T1\rho$ is robust enough to substitute for standard contrast-based methods such as LGE and ECV. The $T1\rho$ approach is deemed successful in this study if it detects elevations detected by a contrast-enhanced image.

2 Method

Pre-reconstructed in vivo CMRs of 41 patients were used in this study. These MRIs were performed on a 1.5 T Siemens scanner. The field of view ranged from 360 to 500 mm. The in-plane resolution was between 1.40-1.95 mm. The data set in this study included image maps ECV, T2 and $T1\rho$. Specifically, the spin-lock frequencies for $T1\rho$ were at 500 Hz, while the spin-lock time was in 10 ms steps, performed for a total of 40 ms. The software *Segment Research* by Medviso [18] was used to analyze the CMR.

2.1 Data Acquisition through Segmentation

Semi-automated 16-part segmentation, based on a modified 17-segment AHA model [14], was performed with the built-in bullseye plot tool in the *Segment Research* [18]. A perpendicular line through the center of the septum was marked as a reference for the software. Furthermore, the epicardial border was eroded inward by 10% and the endocardial outward by 10% to exclude blood pools.

Mean measurements in each segment were calculated by the software [18], using the bullseye plot feature. These mean values were then gathered as tuples of ECV, $T1\rho$ and T2 (in given order) values in a Python dictionary mapped to a specific heart segment in each patient. Afterward, three scatter plots were created when comparing two maps' values at a time: ECV vs. $T1\rho$, T2 vs. $T1\rho$, and ECV vs. T2. The scatter plots were analyzed using pearsonr in Python, from which a correlation coefficient, r, was obtained.

A list of 16 patients, out of the 41 prior, had elevations in the LGE map, which was classed as LGE-positive (LGE+). This acted as another filter. The list was used after segmentation to avoid observation bias. Additionally, data point pairs were filtered out if one of the elements came from an empty cell and, therefore, became a NaN. The number of data points in the scatter plots was counted by computing the length of the arrays derived from the dictionary.

2.2 Data Acquisition through Regions of Interest

Standard deviations and regions of interest (ROIs) were another way to assess the effectiveness of $T1\rho$ in diagnosing myocardial fibrosis. LGE ROIs were marked when suspected collagen highlights were present across 70 unselected patients. These 70 patients were not the same as the 16 above-mentioned LGE-positive patients, although they were also LGE-positive (LGE+). This meant that they had elevations in LGE values, but a clear diagnosis of myocardial fibrosis had not been established. They were compared to a separate marked region of remote healthy tissue of equal size. The masks were then overlaid onto $T1\rho$ maps of the corresponding slice. Afterward, a mean remote healthy tissue value was calculated for the $T1\rho$ remote healthy tissue. Each $T1\rho$ whose ROI mean exceeded the mean of the remote healthy tissue by at least four standard deviations, was counted as an elevation detection. The number of patients with elevations detected by $T1\rho$ was divided by the number of LGE elevations. The quotient was converted to a percentage.

3 Results

Across the 70 LGE-positive patients, $T1\rho$ detected 85% of the elevations that LGE identified. This means that 85% of the $T1\rho$ ROIs were four standard deviations above the mean of remote healthy $T1\rho$ tissue.

The scatter plots below display how the maps correlate with each other. $T1\rho$ values are compared with T2 and ECV values respectively. T2 and ECV values are also compared. Statistical analyses are displayed in tables beneath each subsection. Lowercase r is the Pearson correlation coefficient.

3.1 Results for scatter plots for values based on all patients

The statistical results for the scatter plots for values based on 41 patients are shown in Figure 4, 5, and 6. These statistics are also shown in Table 1 and apply to values of ECV versus $T1\rho$, T2 vs. $T1\rho$, and ECV vs. T2 respectively.

Figure 4 included an ECV vs. $T1\rho$ comparison with 656 data points, where r = 0.194.

Figure 5 had 608 data points for T2 vs. $T1\rho$ values, which yielded r = 0.480. Figure 4 included 608 data points for ECV vs. T2 values, which gave r = 0.340.

Table 1: This table shows the statistics on map value comparison between maps, based on all 41 patients' mean values on the 16 heart segments. Lowercase r is the correlation coefficient. Variable n is the number of paired data points in the scatter plot.

	r	n
ECV vs. $T1\rho$	0.194	656
T2 vs. $T1\rho$	0.480	608
ECV vs. T2	0.340	608

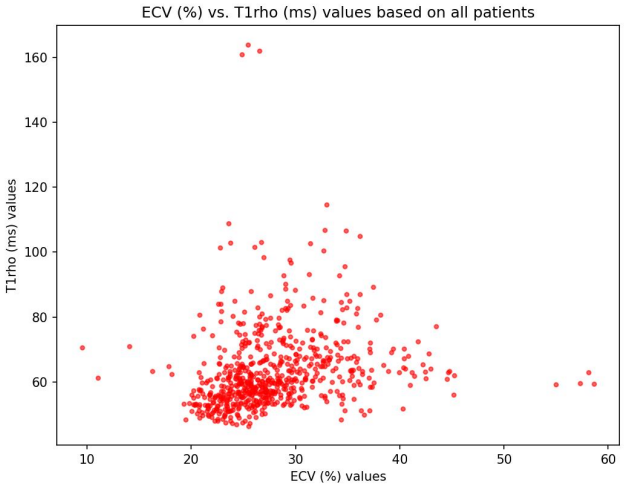

Figure 4: This figure displays a scatter plot with 656 paired data points, where the correlation coefficient r = 0.194. Each data point has the coordinates (x: ECV value, y: $T1\rho$ value) for the same heart segment, in the same slice.

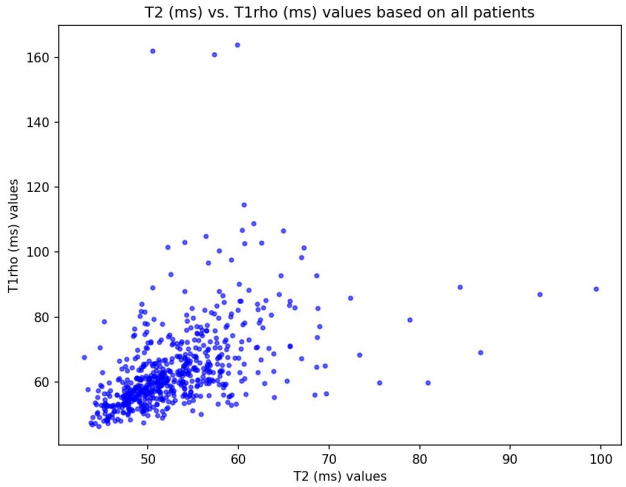

Figure 5: Here, the figure shows a scatter plot with 608 paired data points, with the correlation coefficient r = 0.480. Each data point has the coordinates (x: T2 value, y: $T1\rho$ value) for the same heart segment, in the same slice.

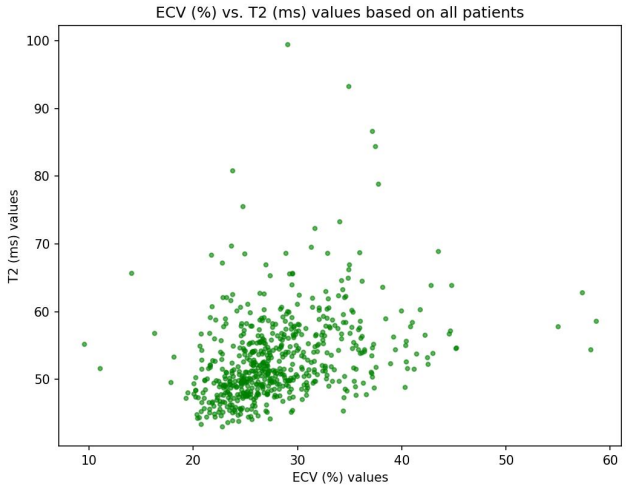

Figure 6: The figure shows a scatter plot between ECV and T2 values with 608 paired data points, with the correlation coefficient r = 0.340. Each data point has the coordinates (x: ECV value, y: T2 value) for the same heart segment, in the same slice.

3.2 Results for scatter plots of all LGE-positive (LGE+) patients' values

The statistical results for the scatter plots for values based on the 16 LGE-positive patients are shown in Figure 7, 8, and 9. These statistics are also shown in Table 2 and apply to values of ECV versus $T1\rho$, T2 vs. $T1\rho$, and ECV vs. T2 respectively.

Each figure used 240 data points. Figure 7 shows ECV compared with $T1\rho$ values, which gave the Pearson correlation coefficient r = 0.047. Next, Figure 8 shows a comparison between T2 and $T1\rho$ values, where r = 0.478. Figure 9 displays ECV compared to T2 values, which produced r = 0.322.

	r	n
ECV vs. $T1\rho$	0.047	240
T2 vs. $T1\rho$	0.478	240
ECV vs. T2	0.322	240

Table 2: This table shows the statistics on map value comparison between maps, based on all 16 LGE-positive patients' mean values on the 16 heart segments. Lowercase r is the correlation coefficient. Variable n is the number of paired data points in the scatter plot.

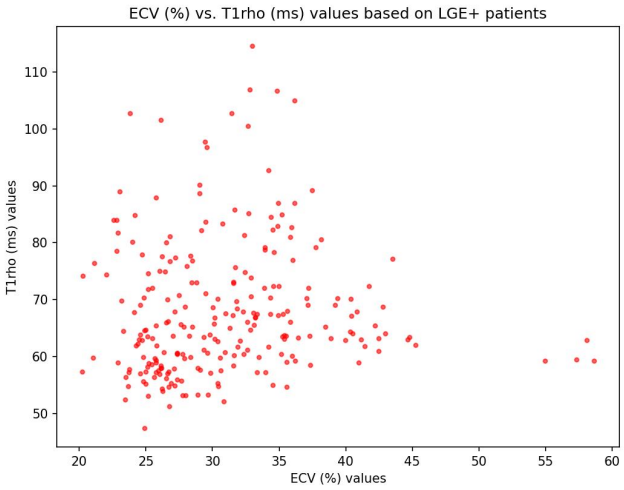

Figure 7: The figure displays a scatter plot with 240 paired data points of T2 and $T1\rho$, where the correlation coefficient r = 0.047. Each data point has the coordinates (x: ECV value, y: $T1\rho$ value) for the same heart segment, in the same slice.

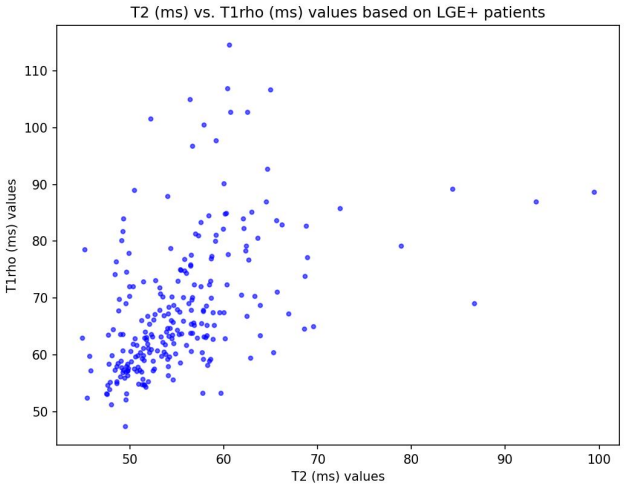

Figure 8: Here, the figure displays a scatter plot with 240 paired data points of T2 and $T1\rho$, where the correlation coefficient r = 0.478. Each data point has the coordinates (x: T2 value, y: $T1\rho$ value) for the same heart segment, in the same slice.

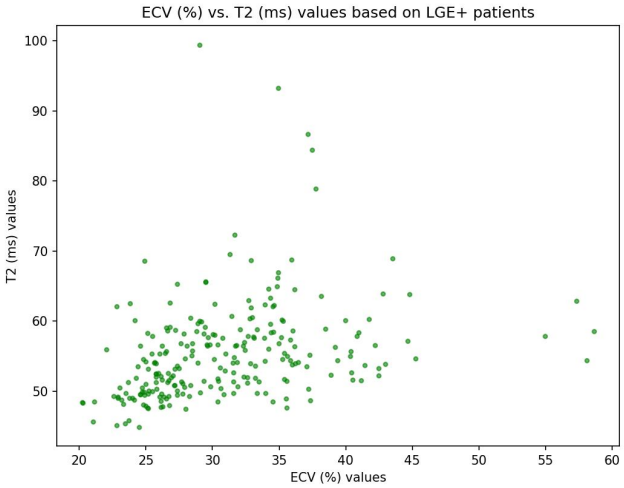

Figure 9: This figure shows a scatter plot with 240 paired data points of ECV and T2, with the correlation coefficient r = 0.322. Each data point has the coordinates (x: ECV value, y: T2 value) for the same heart segment, in the same slice.

4 Discussion

The analysis on the regions of interest (ROIs) showed that $T1\rho$ identified most of the elevations detected by LGE maps. However, segment-wise correlations revealed that the ECV, $T1\rho$ and T2 maps do not measure elevation identically.

4.1 Interpretation of Results

LGE is a valid method for diagnosing myocardial fibrosis [4]. The fact that $T1\rho$ detected 85% of the elevations that LGE identified, indicates that $T1\rho$ is nearly as accurate as LGE in detecting elevations, and thereby indicating possible myocardial fibrosis. However, this 85% sensitivity alone does not establish diagnostic accuracy.

The scatter plots indicated that ECV, T2 and $T1\rho$ did not all vary the same way; therefore, they may not detect the same elevations. This is reflected in the weak correlations (Tables 1 and 2), where none of the correlation coefficients exceeded an absolute value of 0.5.

It is not established, however, how accurately any of the maps can diagnose myocardial fibrosis, since the patients in the data set were unselected. Although in T1, elevation is a marker of myocardial fibrosis, an elevated value is not specific to it, since many conditions raise these values [19].

The scatter plot between ECV and $T1\rho$ yielded a weaker correlation than between T2 vs. $T1\rho$. This comparison can indicate that $T1\rho$ detects similar elevations to those of T2, which makes it more similar to T2 than ECV in what it can detect. This is consistent with what the $T1\rho$ and T2 measure: they are closely related transverse-relaxation measurements, but the spin-lock RF pulse makes $T1\rho$ more sensitive to water-macromolecule interactions [7, 8].

Since an elevation, however, does not always equal fibrosis [19], it is unclear whether using $T1\rho$ over T2 has an advantage in diagnosing myocardial fibrosis.

The correlation between ECV and T2 was weak, but consistently stronger than for ECV vs. $T1\rho$, and weaker than T2 vs. $T1\rho$. This indicates that ECV may still detect elevations that T2 does not, or vice versa. None of these methods is the standard way to diagnose myocardial fibrosis, but rather, LGE is [4]. Therefore, one cannot assume that ECV always detects elevation better than other methods, based on these scatter plots, even though it is a contrast-based method.

There are two possible explanations for the weak correlations between maps. The first is that, since these maps contain different measurements, they should not be expected

to correlate linearly, as the Pearson coefficient r assumes. For example, ECV measures extracellular volume [13], whereas T2 varies based on water content and can indicate inflammation [11]. Further, $T1\rho$ captures microscopic changes in tissue structure [15]. The second explanation is that outliers in the scatter plots created a weak correlation. These outliers could have been caused by blood pools surrounding and within the myocardium, which yielded high values in Figure 1 approaching 150 ms for $T1\rho$. Since bullseye plots compute the mean for a segment, the blood pools may have been included.

The correlations between T2 and $T1\rho$, and ECV and T2 remained similar when patients were filtered based on LGE positivity. However, the correlation between ECV and $T1\rho$ maps weakened when solely LGE-positive patients' CMRs were analyzed. This indicates that for LGE-positive patients, ECV and $T1\rho$ differ more than when all 41 patients were included, in detecting elevations. This may be because fewer healthy patients remained in the scatter plot, and healthy values cluster within a narrow interval [11, 13] [17] (as presented at ISMRM May 2026). The LGE-negative patients without elevations created a more centralized area in the plot. However, filtering them out to only include patients with elevations led to fewer data points and more widespread values.

4.2 Limitations

A limitation in the study is that the 16-segmentation based on the 17-segment AHA-model [14] was performed semi-automatically. Since the user was prompted to mark the center of the septum once for multiple slices, segmentation may have been performed incorrectly by the software if each slice slightly rotated, for example from movement of the scanned patient. This leads to the incorrect segment of the heart being displayed as another in bullseye plot data. Additionally, this study could not standardize the manual marking of the center of the septum, since the position of the mark could not be transferred between image stacks. This could have led to the segmentation between stacks being shifted. If a segment occured, a segment that might have contained myocardial fibrosis would not have been displayed as such in the bullseye plot. Instead, it might have appeared healthy, which would invalidate the accuracy of $T1\rho$ in detecting elevations.

Another limitation is that blood pools might have been included in manual isolation of the left ventricle. This potentially contributed to inflated values in T2, $T1\rho$ and ECV, creating outliers and leading to inaccurate correlation coefficients for establishing robustness in $T1\rho$ detecting elevations for potential diagnosis of myocardial fibrosis. In the data set, the apical slices typically had high values because of blood pools.

4.3 Comparison with Past Studies

To evaluate a proposed motion correction technique for $T1\rho$ MRI maps, Bustin et al. (2021) also used ECG-triggered, bSSFP breath-held MRIs, as was done in this study. They also compared the $T1\rho$ maps to LGE maps.

What Bustin et al. (2021) did differently was in using LGE as a reference for $T1\rho$ remote and injured regions of interest (ROIs), while this study used both ECV and LGE as the reference contrast-based maps, although only LGE for the ROIs. Furthermore, this study used segmentation and mean values per segment to create scatter plots for multi-modal comparison.

Additionally, this study had unselected myocardial fibrosis patients, while Bustin et al. (2021) had selected patients [20]. Bustin et al. (2021) analyzed MR images of 23 patients with suspected myocardial fibrosis, with 15 of them being LGE-positive. This current study did not sort patients based on diagnosis or suspected diagnosis. Rather, one way the patients of this study were sorted was by filtering by LGE-positive patients, meaning patients with MRIs that yielded elevations in LGE maps.

Despite the difference between number of patients, the LGE-positive comparison with $T1\rho$ ROIs yielded similar results. In this study on LGE-positive patients, 85% of ROIs in the $T1\rho$ maps were four standard deviations above the mean remote healthy tissue. The study by Bustin et al. (2021) [20] yielded that $T1\rho$ maps had 93% sensitivity, i.e., were able to detect myocardial injury through elevated values, compared to LGE maps, which support the result of this current study.

In a different study by Oorschot et al., scatter plots and the correlation coefficient r were calculated based on marked ROIs from ECV and $T1\rho$ maps [21]. The correlation

coefficient was 0.66, which is a stronger correlation than in this study (ranging from 0.047 to 0.194). This shows that mean values from segmentation, as in this study, can yield weaker correlations.

4.4 Potential to Expand through Future Research

In a future study, access to a larger sample size, i.e., patient MRI scans, would give a more conclusive answer to the question: can T1ρ be used as a substitute for injection of contrast agents in patients for MRIs? More data points would give a stronger claim on the correlation, which would yield a more reliable conclusion on whether $T1\rho$ can find the same elevations that ECV does.

To minimize the effects of blood in the mean measurement for a given segment, in a future study the epi- and endocardial borders should be shifted more, for example by 15% or 20%. This should be done while keeping the currently marked myocardium data. If the outliers disappear, it would mean that the myocardial borders were drawn too far outside the true myocardium, and therefore included too much blood. To further eliminate outlier points caused by presence of blood, apical slices could be ignored for each image stack per map. However, scar tissue may be present in those apical slices, which would decrease the data set with possible elevations.

In another future study, possible sex-related variations in $T1\rho$ values could be taken into account, like C. Han et al. did [22]. Patient sex could have been extracted from the patient MRI meta data and could establish mean fibrotic tissue values in the ECV, T2 and $T1\rho$ mappings, if patients with myocardial fibrosis had been selected.

To expand on the multi-modal comparison, a comparison with the T1 relaxation mapping should be included. This would give a more definitive picture on how $T1\rho$ compares with established methods, once $T1\rho$ detects elevations more frequently.

Marking Regions of Interest (ROIs) in each map in the myocardium could be a more accurate way to detect possible myocardial fibrosis, over computing mean values per segment, like in this study. The ROIs could be overlaid over different mappings of the same slice to compare how effective $T1\rho$, for example, detects the elevation relative to

LGE: a valid tool for establishing the diagnosis [4]. These ROIs could also be compared to remote healthy tissue, where a factor of increase could be calculated when dividing the mean ROI value with the remote healthy tissue mean value, to establish how clearly the fibrotic tissue is visible between mappings.

The marking of ROIs could, however, include observer bias. This bias could incorrectly yield greater or lesser robustness in the use of $T1\rho$ as an alternative for GBCAs.

Finally, a specificity analysis would further establish the accuracy of $T1\rho$ in diagnosing myocardial fibrosis, rather than only detecting elevations without truly knowing if it indicates myocardial fibrosis, or not. This would be possible if a list of selected patients with diagnosed myocardial fibrosis was given, alongside unselected patients.

4.5 Conclusion

In conclusion, the maps T2, $T1\rho$ and ECV did not always detect the same elevations, as shown by weak correlations: all the correlation coefficients fell within $-0.5 < r < 0.5$. Additionally, although $T1\rho$ appears promising for diagnosis of myocardial fibrosis in the 70 LGE-positive patients, it still needs more work to make it robust enough to replace contrast agents and T2 in clinical settings. This is because of the weaker correlations between $T1\rho$ and ECV maps than between $T1\rho$ and T2, both with LGE-positive and for all patients. The weak correlations could stem from systematic errors in the myocardial segmentation. Moreover, the weak correlations could have been caused by outliers from blood being included in the segmentation. In a future study, the outliers in the scatter plots could be eliminated through removing the slice closest to apex and shifting a percentage greater than 10% of the epicardial and endocardial borders. Finally, more data points would be needed for a fair comparison, since the scatter plots did not all have the same number of points.

AI Use Disclosure

AI never had access to any of the patient images. AI did not access the spreadsheets based on extracted patient data either.

Claude Opus 4.8 at high effort was used to generate Python code to read an imported Excel file with the pandas library and extract data from ECV, $T1\rho$ and T2-mapped MRIs respectively, to put them as values for each key in a dictionary. Each key represents a segment, based on the AHA 16-segment model [14]. One dictionary corresponds to one specific patient. All dictionaries are nested into one larger dictionary that has a key for the patient and a value for the patient data.

Afterward, Claude Opus 4.8 was used to debug the initially human-written Python code meant for creating scatter plots. The bug was that certain array pairs being plotted contained NaNs, because of empty cells in the Excel spreadsheet being analyzed. Because of that, pearsonr in Python could not calculate the correlation coefficient nor statistical significance. Additionally, each array in the pair had to be of the same length. That is why the code eliminates a pair of elements in the array if at least one is a NaN.

Consequently, Claude Opus 4.8 had changed the remaining human-written scatter plot code by rewriting it into a function that could be reused for more multi-modal comparisons, instead of having multiple, unique code blocks that could only be used for one specific scatter plot.

Additionally, Claude Opus 4.8 fixed a major bug in the code for creating scatter plots. Only ECV values below 31% were supposed to be filtered out, but instead the code would filter out any mapping if it was in the x-position, which was the case for the T2 vs $T1\rho$ plot initially. Claude Opus 4.8 implemented safeguard to check if the name of the x-label is ECV and not a different mapping. In this study, the ECV mapping is never the y-label for the scatter plots.

Claude Opus 4.8 was used to generate LaTeX code to format Figure 1 to place the images next to each, without gaining access to the images themselves.

References

[1] E. Asadollahzade, F. Ghadiri, Z. Ebadi, and A. N. Moghadasi, "The benefits and side effects of gadolinium-based contrast agents in multiple sclerosis patients," 2022.

[2] B. Ambale-Venkatesh and J. A. Lima, "Cardiac mri: a central prognostic tool in myocardial fibrosis," *Nature reviews cardiology*, vol. 12, no. 1, pp. 18–29, 2015.

[3] H. A. BaniHani, L. H. Khaled, N. M. Al Sharaa, R. A. Al Saleh, A. K. B. Ghalaita, A. S. B. Sulaiman, A. Holeihel, *et al.*, "Causes, diagnosis, treatment, and prognosis of cardiac fibrosis: a systematic review," *Cureus*, vol. 17, no. 3, 2025.

[4] G. D. Aquaro, C. De Gori, L. Faggioni, M. L. Parisella, D. Cioni, R. Lencioni, and E. Neri, "Diagnostic and prognostic role of late gadolinium enhancement in cardiomyopathies," *European Heart Journal Supplements*, vol. 25, no. Supplement_C, pp. C130–C136, 2023.

[5] M. Jerosch-Herold and R. Y. Kwong, "Magnetic resonance imaging in the assessment of ventricular remodeling and viability," *Current heart failure reports*, vol. 5, no. 1, pp. 5–10, 2008.

[6] D. Ripley, T. Musa, L. Dobson, S. Plein, and J. Greenwood, "Cardiovascular magnetic resonance imaging: what the general cardiologist should know," *Heart*, vol. 102, no. 19, pp. 1589–1603, 2016.

[7] A. Bustin, W. R. Witschey, R. B. van Heeswijk, H. Cochet, and M. Stuber, "Magnetic resonance myocardial t1ρ mapping: Technical overview, challenges, emerging developments, and clinical applications," *Journal of Cardiovascular Magnetic Resonance*, vol. 25, no. 1, p. 34, 2023.

[8] T. F. Ismail, W. Strugnell, C. Coletti, M. Božić-Iven, S. Weingaertner, K. Hammernik, T. Correia, and T. Kuestner, "Cardiac mr: from theory to practice," *Frontiers in cardiovascular medicine*, vol. 9, p. 826283, 2022.

[9] R. D. Graaf, *In Vivo NMR Spectroscopy: principles and techniques*. John Wiley & Sons Ltd., 3 ed., 2019.

[10] A. G. Raafs, B. P. Adriaans, M. T. Henkens, J. A. Verdonschot, M. J. Ramaekers, S. Gommers, M. A. Abdul Hamid, S. Schalla, C. Knackstedt, V. P. van Empel, *et al.*, "Myocardial fibrosis assessment using t1 and ecv mapping with histologic validation in chronic dilated cardiomyopathy," *Cardiovascular Imaging*, vol. 15, no. 10, pp. 1828–1830, 2022.

[11] P. K. Kim, Y. J. Hong, D. J. Im, Y. J. Suh, C. H. Park, J. Y. Kim, S. Chang, H.-J. Lee, J. Hur, Y. J. Kim, *et al.*, "Myocardial t1 and t2 mapping: techniques and clinical applications," *Korean journal of radiology*, vol. 18, no. 1, pp. 113–131, 2017.

[12] Y. Amano, M. Tachi, H. Tani, K. Mizuno, Y. Kobayashi, and S. Kumita, "T2-weighted cardiac magnetic resonance imaging of edema in myocardial diseases," *The Scientific World Journal*, vol. 2012, no. 1, p. 194069, 2012.

[13] P. Kellman, J. R. Wilson, H. Xue, W. P. Bandettini, S. M. Shanbhag, K. M. Druey, M. Ugander, and A. E. Arai, "Extracellular volume fraction mapping in the myocardium, part 2: initial clinical experience," *Journal of Cardiovascular Magnetic Resonance*, vol. 14, no. 1, p. 61, 2012.

[14] A. H. A. W. G. on Myocardial Segmentation, R. for Cardiac Imaging:, M. D. Cerqueira, N. J. Weissman, V. Dilsizian, A. K. Jacobs, S. Kaul, W. K. Laskey, D. J. Pennell, J. A. Rumberger, T. Ryan, *et al.*, "Standardized myocardial segmentation and nomenclature for tomographic imaging of the heart: a statement for healthcare professionals from the cardiac imaging committee of the council on clinical cardiology of the american heart association," *Circulation*, vol. 105, no. 4, pp. 539–542, 2002.

[15] N. Prapan, T. Songsangjinda, S. Phoopattana, P. Tanapibunpon, S. Breil, P. Sangpin, S. Zhang, and R. Krittayaphong, "Native t1-rho mapping for myocardial scar detection in patients with probable or confirmed coronary artery disease," *Quantitative Imaging in Medicine and Surgery*, vol. 16, no. 1, p. 1, 2026.

[16] T. Liu, D. Song, J. Dong, P. Zhu, J. Liu, W. Liu, X. Ma, L. Zhao, and S. Ling, "Current understanding of the pathophysiology of myocardial fibrosis and its quantitative assessment in heart failure," *Frontiers in physiology*, vol. 8, p. 238, 2017.

[17] P. Pandurevic, J. Castaings, J. Nickander, and A. Fyrdahl, "Myocardial t1rho mapping at 1.5 t: Normal values and initial patient experience," in *Cape Town - 2026 ISMRM-ISMRT Annual Meeting and Exhibition*, (Cape Town, South Africa), ISMRM, May 2026. Program Number: 467-02-004.

[18] Medviso, "Segment research." `https://medviso.com/segment/`, Release date unknown.

[19] R. J. Perea, J. T. Ortiz-Perez, M. Sole, M. T. Cibeira, T. M. de Caralt, S. Prat-Gonzalez, X. Bosch, A. Berruezo, M. Sanchez, and J. Blade, "T1 mapping: characterisation of myocardial interstitial space," *Insights into imaging*, vol. 6, no. 2, pp. 189–202, 2015.

[20] A. Bustin, S. Toupin, S. Sridi, J. Yerly, O. Bernus, L. Labrousse, B. Quesson, J. Rogier, M. Haïssaguerre, R. van Heeswijk, *et al.*, "Endogenous assessment of myocardial injury with single-shot model-based non-rigid motion-corrected t1 rho mapping," *Journal of Cardiovascular Magnetic Resonance*, vol. 23, no. 1, p. 119, 2021.

[21] J. W. van Oorschot, F. Güçlü, S. de Jong, S. A. Chamuleau, P. R. Luijten, T. Leiner, and J. J. Zwanenburg, "Endogenous assessment of diffuse myocardial fibrosis in patients with t1ρ-mapping," *Journal of Magnetic Resonance Imaging*, vol. 45, no. 1, pp. 132–138, 2017.

[22] C. Han, H. Xu, H. Gao, F. Liu, J. Wu, Y. Liu, Y. Cheng, W. Deng, X. Yue, Z. Wu, *et al.*, "Effect of spin-lock frequency on quantitative myocardial t1ρ mapping," *Insights into Imaging*, vol. 15, no. 1, p. 176, 2024.